Bioactive Silk Protein Biomaterial Systems for Optical Devices

Brian D. Lawrence,[†] Mark Cronin-Golomb,[†] Irene Georgakoudi,[†] David L. Kaplan,[†] and Fiorenzo G. Omenetto*[,†,‡]

Department of Biomedical Engineering and Department of Physics, Tufts University, Science and Technology Center, 4 Colby Street, Medford, Massachusetts 01225

Received November 10, 2007; Revised Manuscript Received February 12, 2008

Silk-based biomaterial systems have been previously explored for a variety of medical and nonmedical materials needs. The unique biophysical features of silks provide options to generate highly tailored structures and morphologies with this unique family of fibrous proteins. To exploit these features, we have optimized the all aqueous processing of silk fibroin into novel surface nanopatterned protein materials. We have exploited control of this nanomorphology to optimize the optical features of these silk protein systems. We demonstrate control of surface morphology down to 125 nm, with fidelity over large length scales. This surface nanopatterning allows the silk protein to be formed into diffractive optics such as diffraction gratings, pattern generators, and lenses due to novel aqueous processing into optically clear materials via control of β sheet crystallinity. Further, we incorporate biological components, such as hemoglobin and the enzyme peroxidase, during the process of forming the silk diffraction gratings. The ambient processing of the silk protein in water, in combination with these bioactive components, allows these entrained molecules to retain activity and provide added functions and selectivity to the optically active silk films. Thus, combinations of biochemical and optical readout is feasible and provides in a single, disposable/all degradable element with both spectral discrimination and biological function. These new surface nanopatterned, bioactive silk protein-based material systems offer a unique combination of features potentially useful for a range of biosensor needs, particularly when considered in concert with the remarkable mechanical properties of these proteins, their biocompatibility, and controllable biodegradation.

Introduction

Current optical device platforms are based primarily on glass, semiconductors or polymers, and are used to generate complex functional features in these systems. However, the harsh processing requirements, as well as the lack of biocompatibility and biodegradability features of these materials, limit some important areas of potential utility, such as implantable degradable systems, to avoid having to surgically remove the device postfunctional lifetime, the use of such sensors for broad environmental distribution where the lack of degradability would cause environmental contamination post use, and the inability to functionalize the devices with bioactive sensing components due to the solvents and temperatures used in processing. Thus, new approaches are needed to overcome these limitations while still retaining the useful material robustness and optical features of current devices. Toward this goal, biologically inspired interfaces have been the subject of recent attention with efforts devoted to understanding and mimicking naturally occurring systems. Particular focus has been directed at biologically inspired photonic elements, which provide sophisticated optical processing, sensitivity and transduction in living matter.[1,2] This area of research has been enabled by soft lithography with elastomers, such as polydimethylsiloxane (PDMS), which offer the ability for detailed reproduction at the micro- and nanoscales of morphologies and patterns that accompany functional, naturally occurring optical systems. The idea of integrating optical readout and biological function in a single element has been recently emerging in applications that use hydrogel-based active holograms.[1]

Natural biopolymers can offer further advantages given the favorable processing conditions, often at ambient temperature, which would allow the direct inclusion of biological dopants during biopolymer processing and cross-linking. Furthermore, biopolymers offer more favorable opportunities for biocompatibility and biodegradability in comparison to inorganic polymers. Silk fibroin is a particularly interesting candidate with which to explore the integration of optical and biological function in a single element by offering all-aqueous processing, ease of functionalization, and the ability to generate optically relevant morphologies such as ultrathin films, thick films, nanoscale, and large diameter fibers.[2–4] Additionally, these films are mechanically robust,[5] in contrast to other biopolymers, and present excellent surface quality and transparency. Silk proteins represent a unique family of biopolymers due to their novel structure, biology, and remarkable material properties.[2–4] From a materials science perspective, silks spun by spiders and silkworms represent the strongest and toughest natural fibers known and offer many opportunities for functionalization, processing, and biological integration when compared to conventional polymers.

Silk fibroin film patterning on micrometer length scales with modified soft lithography approaches was recently reported using ionic salt solution processing.[6] Optical devices that are mechanically robust yet fully biodegradable and biocompatible are not available today. Such systems would greatly expand the utility of current optical platforms into a broader range of medical and environmental fields, areas currently limited to retrievable devices. Thus, the goal of the present study was to study the formation of optically active silk-based materials with a focus toward biosensor needs. Toward this goal, a novel optics platform is described based on exploiting the unique mechanical

* Corresponding author. E-mail: fiorenzo.omenetto@tufts.edu.
[†] Department of Biomedical Engineering, Tufts University, Science and Technology Center.
[‡] Department of Physics, Tufts University, Science and Technology Center.

10.1021/bm701235f CCC: $40.75
Published on Web 03/28/2008

and processing features of silk fibroin proteins. This system can be prepared in an all-aqueous approach, allowing the direct incorporation of reactive biological components in the devices to add selective functions. The materials can be prepared with optical clarity and with surfaces reshaped for optical interface and readout by writing diffractive elements such as diffraction gratings, microlens arrays or pattern generators. For the direct utilization in optical detection modes, the systems are mechanically durable as tough biomaterials, and the systems will fully biodegrade over weeks to years depending on the mode of preparation.[7,8] The successful demonstration of the bio-optical utility of these novel systems suggests an entirely new window of opportunity in environmental and medical sensor platforms that can not be met with current optical material and device platforms. This window of application is achieved due to the novel combination of essential features of mechanics, optics and biological compatibility with the system described in this report.

Methods

Solution Preparation. The silk solution was obtained by boiling *Bombyx mori* cocoons for 30 min in an aqueous solution of 0.02 M Na_2CO_3, then rinsed thoroughly with water to extract the gluelike sericin proteins, using methods we have previously reported.[4] The solution was then dissolved in 9.3 M LiBr solution at room temperature, yielding a 20 wt % solution. This solution was dialyzed in water using a dialysis cassette with a molecular cutoff weight of 3500 Da for 48 h.

Film Preparation. The silk fibroin solutions were poured onto polydimethylsiloxane (PDMS) negative molds of ruled and holographic diffraction gratings (Edmund Optics, Barrington, NJ) with 600, 1200, 2400, and 3600 grooves/mm spacing. The cast silk solution was then set to air-dry in a laminar flow hood. The films were then left to dry for 24 or 48 h until all the solvent had evaporated to give solid fibroin protein silk films. After drying, the films were mechanically removed by using a surgical blade to lift one corner of the solidified film from the patterning mask. This corner was then raised and lifted off the grating surface using forceps. Different film thicknesses were obtained indeed by varying the weight %/vol protein concentration used during casting. The dependence between the concentration and the resulting film thickness is illustrated in Figure 3e.

The films were then placed in a water vapor environment, exposed to a high humidity atmosphere at room temperature.[8] The films were water annealed for two hours or longer, depending on the preparation, and based on our prior water-annealing techniques for these materials to improve materials handling characteristics.[8] The films were then removed form the high humidity atmosphere, allowed to dry overnight in a laminar flow hood, and then sectioned for optical evaluation. The lenses, microlens arrays and 64-phase level 2D diffraction patterns were realized by casting the silk solution following the same protocol described above, but on polycarbonate micro and nanopatterned masters (Digital Optics, Tessera Inc., San Jose, CA).

Diffracted spectra and patterns were obtained by propagating a supercontinuum white light laser source[9] through the silk optical elements and by recording an image in the far field on a screen placed ~10 cm from the optical element.

Physical Characterization. Scanning electron microscopy (SEM) was used to assess silk film cross-sectional thickness. Cast silk film samples were water-annealed for 12 h, then frozen in liquid nitrogen, and cracked using a razor. The films were then mounted on an aluminum block vertically with conductive tape and then sputter coated with gold using a Polaron SC502 sputter coater (Fisons,VG Microtech, East Sussex, England). The films were then imaged using a JEOL JSM-840 scanning microscope (JEOL Ltd., Tokyo, Japan). Image analysis software (ImageJ, National Institutes of Health) was used to determine silk film cross-sectional thickness. Field emission scanning electron microscopy (FE-SEM) was used to determine surface patterning

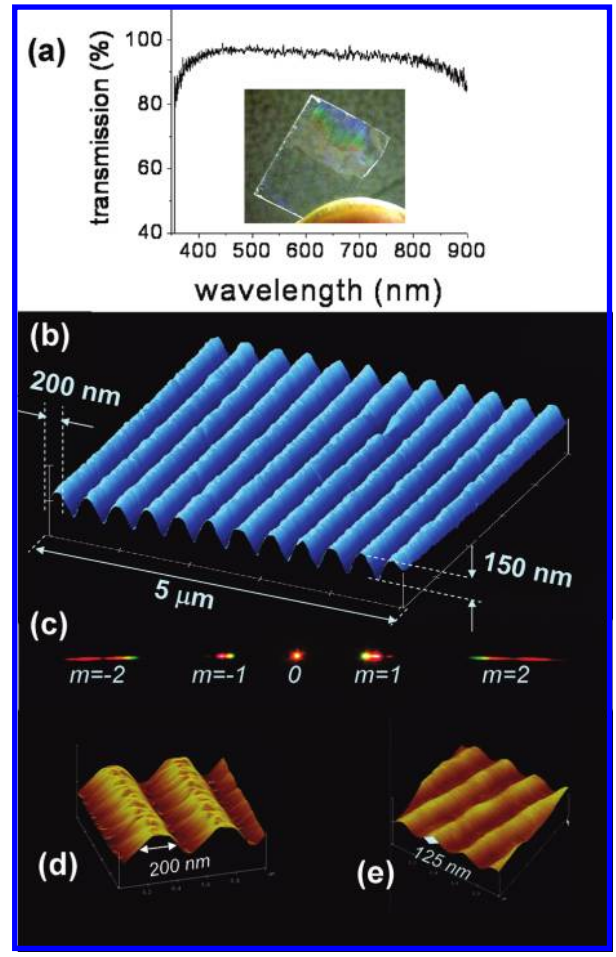

Figure 1. (a) Measured transparency curve of a 50 μm thick silk film and picture of a silk film, (b) a nanopatterned optical element from silk with an AFM image of a 2400 line/mm silk grating. (c) Diffracted orders from the propagation of a white light laser source (supercontinuum laser source) through the silk grating. The diffracted orders are imaged ~10 cm from the grating. (d,e) AFM images of smaller sections of the 2400 and 3600 lines/mm silk gratings, respectively. The sections measure 1 μm^2 and show a peak to valley height difference of 150 and 60 nm, respectively. The topographic analysis obtained from these measurements have yielded a surface roughness of less than 10 nm rms.

topography upon the silk films. Silk film samples were first water-annealed in a vacuum for 12 h, and then sputter coated with gold using a Polaron SC502 sputter coater (Fisons,VG Microtech, East Sussex, England). The samples were then imaged using a LEO 982 FE-SEM (LEO Electron Microsopy, Inc., Thornwood, NY). Groove width measurements we determined with ImageJ analysis software.

Atomic force microscopy (AFM) was used to determine groove depth and surface roughness of the patterned silk films. Silk films samples were water-annealed for 12 h. Images of the film samples were acquired with a Digital Instrument Dimension 3100 (Veeco Instruments, Inc., Woodbury, NY) in tapping mode. Images were taken in air, flattened, and plane fitted as required.

A Metricon waveguide instrument was used to evaluate the film thickness and the index of refraction of the silk films. The measured indices of refraction and film thicknesses are evaluated at a wavelength of $\lambda = 633$ nm. Diffraction efficiency was measured with calibrated thermopile power meters (Molectron, Portland, OR).

Both patterned and nonpatterned silk fibroin films were evaluated using a Bruker Equinox 55/S FT-IR spectrometer (Bruker, Billerica, MA). Spectral scans were obtained using dehydrated samples of both untreated and water-annealed silk films. Each spectrum was acquired over the range of 4000–400 cm^{-1} for 66 scans with a resolution of 4 cm^{-1}.

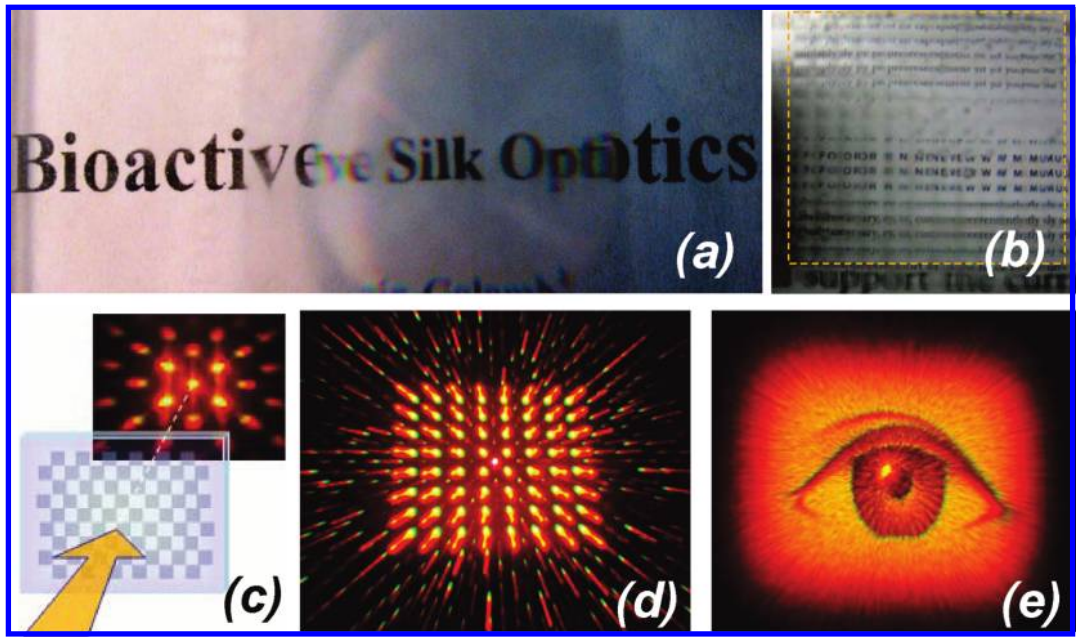

Figure 2. Different silk optical elements. The image shows the realization of a (a) a silk lens, (b) a 12 × 12 silk lens array. (c) Schematic showing the approach to generate images (d) and (e) where different projected patterns are obtained from propagation of a white light laser source through 2D, 64 phase level diffraction patterns. The images are taken in the far field at a distance of 10 cm from the silk optical element. (masters from Digital Optics Inc., Tessera Corporation).

Functionalization of Films with Bioactive Components. For hemoglobin doped systems, a human blood−silk solution was prepared by combining 1 mL of donated human blood and 5 mL of the 8% silk solution. The red blood cells were used under Tufts University approved human use protocols (031-2005). The mixture was poured on a 600 lines/mm optical grating, and allowed to dry overnight. The following morning the film was removed from the optical grating and water annealed for two hours by placing the grating in a controlled water vapor environment as described above. Samples were then evaluated in oxygenated and deoxygenated solutions to assess retention of function, based on absorption spectra for the two forms of the hemoglobin. The grating was placed in a quartz cuvette filled with distilled water and the absorbance of the solution before and after nitrogen gas bubbling into the cuvette after 15 min was used to assess stability. The assay was run in static mode and with the film placed at the bottom of the cuvette. Red blood cells were used in the present study to optimize potential stability of the hemoglobin, as determined by the spectral signatures in the two states, oxygenated and deoxygenated.

For silk films containing the enzyme peroxidase, the 8% silk solution was combined with peroxidase (Sigma-Aldrich) to give a 0.5 mg/mL concentration of enzyme. The solution was poured on the optical gratings and Teflon surfaces. The films were allowed to dry, and then the optical grating cast films and the coated Teflon films were water annealed for 2 h in the presence of water vapor as described above. These films were then used to assess function of the enzyme by reaction with tetramethylbenzidine (TMB), an aromatic organic monomer that reacts in the presence of hydrogen peroxide to generate a color in the presence of active enzyme via a free radical reaction.[10] The oxidation products of TMB yield a characteristic blue (one-electron oxidation, with peak emission at $\lambda = 450$ nm) and yellow color (two-electron oxidation, with peak emission at $\lambda = 652$ nm), and were used to track enzyme activity in the silk optical gratings. The enzyme content of the films, in terms of total content of active enzyme, can not be readily determined, as the enzyme can not be extracted from the film without loss of function. Thus, activity was determined based on retention of ability to convert the TMB substrate on a time-dependent basis, and not absolute values. Activity was assessed over 45 days, with the film placed at the bottom of a cuvette, the TMB added, and spectroscopic measures taken after a few minutes to allow time for diffusion of reactants into the film.

For the films containing Phenol Red, the 8% silk solution was combined with the pH indicator, Phenol Red (Sigma-Aldrich), to give a 1 mg/mL concentration of indicator. The silk/Phenol Red solution was then cast upon a 600 lines/mm grating (Edmund Optics). The films were dried overnight, and then annealed in the presence of water vapor for two hours. After annealing, the films were removed and placed into prepared buffer solutions with pH's 7 and 10 to assess the impact of pH on film color, mediated by the embedded indicator dye.

Results and Discussion

The formation of nanopatterned silk optical elements was addressed by inducing crystallization of films on appropriate substrates in a similar fashion to soft transfer molding.[4,11] The extracted silk was processed to yield an aqueous solution (8.0 wt % silk), key for generating optically clear materials during film fabrication. The 8 wt % content of silk in these solutions was determined based on gravimetric analysis upon drying samples of the solutions prepared and dialyzed as described earlier. To assess baseline optical properties, the films were obtained by casting the silk solution on smooth substrates (such as a Teflon plate) for ease and even detachment after the transition from the liquid to the solid phase has occurred.

Spectral evaluation showed high transmission (T between 90 and 95%) across most of the visible spectrum (Figure 1). The refractive index of these films is measured with a waveguide instrument and is found to consistently be $n = 1.55$ for various films measured with thicknesses ranging between 30 and 50 μm. All of the films used in this work are free-standing and fall in this thickness range. To generate diffractive optical elements, the silk solution was cast on patterned diffractive optical surfaces, including different holographic diffraction gratings with varying line pitches as masks. Once dried, the films were water annealed for two hours, removed, and allowed to dry. Removal from the grating mask was accomplished by simple mechanical lifting of the grating from the substrate. Upon separation of the master grating from the silk film, the silk diffraction gratings were characterized for surface morphology

by scanning electron and atomic force microscopies. The silk diffractive gratings were very efficient and redirected 37% of the incident light into the first diffracted order. Figure 1 shows the zeroth first and second diffracted orders from a silk grating that was crossed by a supercontinuum source.[9] Parts d and e of Figure 1 show the silk replicated patterns from 2400 and 3600 lines/mm holographic grating masters. The grooves were 200 and 125 nm wide (full width at half-maximum). Upon closer examination of the AFM images, smooth sidewalls on the grating features were observed. An evaluation of the surface roughness at the peaks and valleys of the grooves revealed root-mean-square values below 10 nanometers, which represents outstanding resolution both from the optical and materials perspectives. Gratings as large as 50 mm × 50 mm were realized with this technique.

Similar surface patterning results were reported using 1-butyl-3-methylimidazolium chloride (BMIC) ionic liquid solution,[12] further supporting our finding that silk fibroin produces high resolution surface patterning geometries of the cast surface. Unlike these previous studies however, our methodology is an all-aqueous process, uses casting methods as opposed to spin coating techniques, and does not require methanol for film formation and stabilization. These features are advantageous for the inclusion of labile molecules, such as proteins, organisms and DNA, among others, and also may be advantageous for potential biomedical applications, where residuals from toxic chemicals may be a problem for biological systems. In addition our method for film formation is accomplished through solvent evaporation, and is a highly controllable process for producing desired film dimensions. Furthermore, the crystallinity content can be easily controlled using multiple postcasting processes, which is not as easily accomplished using a methanol induced film formation approach.[4]

The measured diffraction efficiency of these gratings was 34% in the first order at a wavelength of 633 nm, favorably comparing to conventional transmissive glass gratings. To further test the ability to realize optical elements in silk by surface nanopatterning, a variety of transmissive/diffractive optics were successfully manufactured by the same technique, resulting in the formation of silk lenses, microlens arrays, pattern generators or beam reshapers. These different realizations are based on the ability to pattern silk on the nanometer scale in order to realize sophisticated optical functions which can further expand the application space of biologically active optics. Figure 2 illustrates a sample of the silk optical elements that have been generated using the approaches described above. Lenses and microlens arrays can be predesigned and used, for instance, to couple light directly into the biological substrate while 2D diffraction patterns can add more degrees of freedom to programmable optical readout. While the variety and quality of optical elements attainable is of interest from a biomaterials and optical standpoint, the most compelling feature is the fact that they are prepared, processed and optimized in all aqueous environments and at ambient temperature, which offers an important opportunity to include labile biological 'receptors' in the form of proteins or related systems within the solution and to recast the optical elements as biologically active optics that offer new opportunities for sensing.

Film thicknesses from 10 to 100 μm were generated and characterized for transparency and optical quality. For most experiments a standard 100 μm silk film thickness was used. This film thickness was chosen primarily based on ease of handling, film flatness postcasting, and the presence of superior optical clarity, which we have quantified by numerous sample

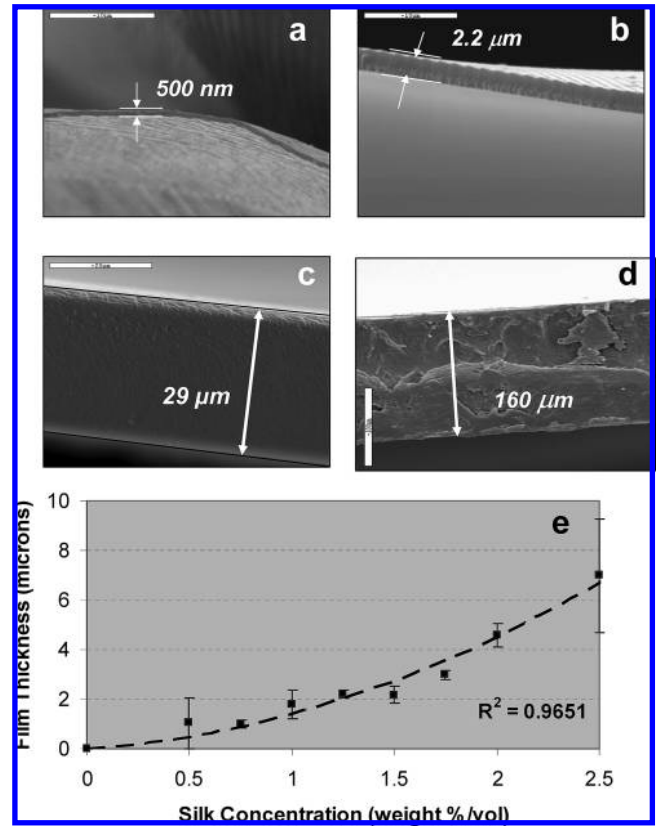

Figure 3. SEM images of silk film cross-sections with varying thicknesses. Films were produced ranging from hundreds of nanometers to hundreds of micrometers in thickness (a−d). The surface patterning was also maintained on all film sizes and can be seen on the thin film cross-sections (a−b). (e) Relationship between the concentration of protein used in solution and the thickness of the silk film obtained.

measurements of transmission across the visible wavelengths and found to approach 100% (accounting for the surface losses). SEM images of silk film cross-sections with varying thicknesses are shown in Figure 3. The surface patterning can also be observed with the cross-sections (a−b).

The films formed in this way were characterized for structural features, as we have previously reported for aqueous processed silk-based materials.[8] The presence of silk fibroin β-sheet structure was observed for the water-annealed silk fibroin films for both patterned and nonpatterned samples based on FT-IR (Figure 4). All of the water-annealed film samples contained a peak in the amide I region near 1630 cm^{-1}, which has been previously shown to indicate the formation of β-sheet structures.[4] β-sheet structure was also confirmed functionally, based on the insolubility of water-annealed films when placed in a water bath. Throughout these experiments, the gratings were found to be noticeably insensitive to fluctuations in the humidity of the laboratory environment and did not show any appreciable structural variation even when immersed in water. Random coil structures were also detected in both the water-annealed and nonannealed films within the amide I region near 1650 cm^{-1} and the amide II region near 1538 cm^{-1}. For the nonannealed silk films there was no peak indicating β-sheet structure formation in the designated amide-I region, and the films were found to be soluble in water. The absence of β-sheet formation was also observed for varying silk film surface groove patterns of 0, 600, 1200, 2400, and 3600 lines/mm, and indicates that the formation of the surface patterns on the silk films did not induce β-sheet structure formation.

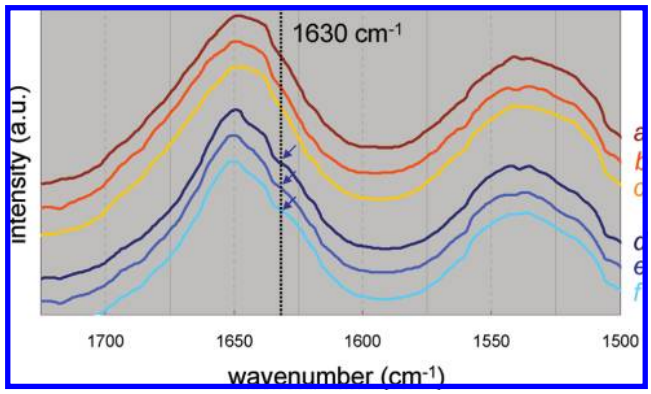

Figure 4. FT-IR spectra for untreated (a−c) and water-annealed (d−f) silk fibroin films. The presence of a slight peak in the amide region around 1630 cm^{-1} for the water-annealed samples indicates silk fibroin β-sheet structure. The presence of silk random coil structure was found in both treatments, as indicated by peaks located near 1538 and 1650 cm^{-1}. Comparing similar processing spectra with changing surface groove number ((a,d) 0 lines/mm, (b,e) 600 lines/mm, and (c,f) 3600 lines/mm) demonstrated that the surface patterning did not affect the formation of β-sheet structure in the films.

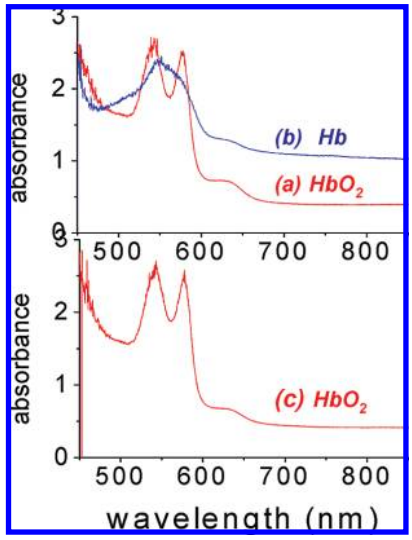

Figure 5. Biologically active silk optical gratings doped with hemoglobin. Hemoglobin immobilized within the optical grating undergoes a transition from the oxygenated state (curve a) to deoxygenated state (curve b) when the optical element is exposed to nitrogen. When nitrogen flow is stopped, the oxyhemoglobin peaks were recovered (c).

The experimental realization and evaluation of these specialized optical elements was investigated by including a variety of biological substances in the aqueous silk solution and subsequently analyzing their functionality within the solidified films. The experiments involved embedding: (a) a physiologically relevant protein (hemoglobin) (Figure 5), (b) an enzyme (horseradish peroxidase, HRP) (Figure 6), and (c) small organic pH indicator (Phenol Red) within the silk optical matrix (Figure 7). All these samples were diluted into the aqueous silk fibroin solution and then cast onto diffractive solid state structures to consolidate the optical properties and the function of the biological dopant. The structural features of the films were found to be consistent, with reproducible thickness and with no appreciable variation in refractive index for the experiments performed here. Control and design of the nanostructured geometry can render the silk diffractive optical element more sensitive to the expected small changes in the index of refraction

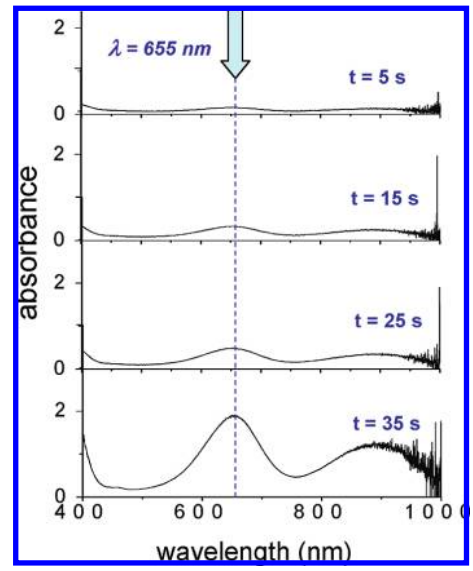

Figure 6. Enzyme active silk optical gratings doped with horseradish peroxidase. The data corresponds to the spectral transition of an enzyme-doped silk optical grating when exposed to TMB for verification of enzyme activity. The presence and increase of the absorbance of the optical element indicates the activity of the enzyme within the optical element.

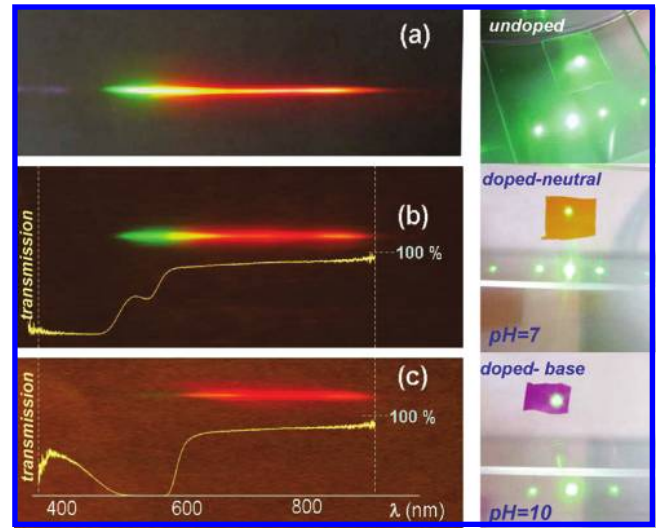

Figure 7. Transmission of white light supercontinuum (SC) from 350 to >1000 nm through a phenolsulfonphthalein (PSP) activated silk optical grating. The spectral images are taken at a distance of 15 cm from the grating. The SC diffracted by an undoped grating and projected onto a fixed plane is illustrated for reference in (a). When the PSP grating is exposed to a neutral solution (b), the spectral absorption of the grating is changed, affecting the diffracted SC spectrum. The measured spectral transmission curve is overlaid to match the diffracted SC spectrum detected. (c) When the PSP grating is exposed to a base solution, more absorbance is exhibited towards the green end of the spectrum, both visible in the measured curve and in the diffracted and imaged SC spectrum. The images on the right show the diffracted orders of the three silk gratings when a monochromatic green laser is propagated through them.

and make use of their variation as a signal. These studies will be the subject of a separate paper.

As a first investigation of substrate biocompatibility, red blood cells (RBCs) were incorporated into the silk grating. The RBC−silk fibroin solutions were prepared by combining 1 mL of an 80% hematocrit human RBC solution and 5 mL of the 8% silk solution. The mixture was cast on a 600 lines/mm

optical grating and allowed to dry overnight. The films were removed from the optical grating and annealed in a water vapor environment for two hours. The grating structure was still present and diffraction orders were observed. The hemoglobin−silk optics was then stored at room temperature and re-evaluated after four days. An optical transmission experiment was then performed to determine whether hemoglobin, the oxygen-carrying protein contained in RBCs, maintained activity within the matrix of the silk optical element. The grating was inserted in a quartz cuvette filled with distilled water. The absorbance curves exhibited two peaks typical of oxyhemoglobin absorption.[13] Subsequently, nitrogen gas was bubbled into the cuvette to deoxygenate hemoglobin and after 15 min the characteristic absorption peaks of oxyhemoglobin disappeared. The results shown in Figure 5 indicate the retention of hemoglobin function within this silk optical grating, further confirmed when the nitrogen flow to the cuvette was halted and the oxyhemoglobin spectral peaks reappeared.

A second active optical element was realized by adding HRP to the silk solution to generate a 0.5 mg/mL concentration of enzyme embedded in the silk film. A variety of chromogens have been used to localize peroxidase in tissue sections. In analogous fashion, to verify enzyme activity, TMB, an aromatic organic monomer that reacts in the presence of hydrogen peroxide to generate a color in the presence of active enzyme via a free radical reaction, was used to track enzyme activity in the silk optical gratings.[10] The oxidation products of TMB yield a characteristic blue (one-electron oxidation) and yellow color (two-electron oxidation). The recorded spectra represent the initial stages of the reaction immediately after exposing the optical element to TMB, along with images of the resulting transition (Figure 6). Measurements were taken up to 45 days after initial preparation of the grating indicating that the HRP was still active in the silk protein matrix. These were relative measures, as the content of protein in active state in the film can not be determined without loss of bioactivity. During the time of study over 45 days, the HRP−silk grating was stored at room temperature; thus no special care was taken to stabilize this enzyme in the film. We have previously reported the immobilization of HRP on silk protein matrices, with successful retention of function, however, in this prior study the enzyme was covalently coupled to the silk to form a gradient of enzyme activity.[14]

To determine the utility of the system for small molecules, an organic pH indicator, phenolsulfonphthalein (Phenol Red), was mixed with the silk protein aqueous solution and cast onto 600 lines/mm gratings. The resulting diffractive optic structures maintained the functionality of the indicator and the optical function of the diffraction grating. This feature was shown by propagating supercontinuum radiation onto the Phenol Red silk grating, where it was diffracted. The same grating was then dipped into solutions with different pH (1 mM NaOH, 1 mM HCl, DI H_2O) and the change in the dispersed spectrum was observed. Variations of the spectrum could be correlated to the acidity of the solutions (Figure 7) where the measured transmission curves are overlaid to the far field images of the diffracted supercontinuum. As in the previous cases, the active silk grating was mechanically sturdy, can be stored at room temperature, can be reused, is reversible, and can be handled like a regular optical element. For example, we recently reported outstanding mechanical properties both in compressive and tensile modes for ultrathin silk films with thickness below 100 nm (Jiang et al., 2007[5]). The films were characterized by high elastic modulus of 6.5 GPa and ultimate tensile strength reaching 100 MPa. These properties were due to the gradual development of the self-reinforcing microstructure of highly crystalline β-sheets, serving as reinforcing fillers and physical cross-links.

Numerous reports have shown that silk fibroin acts as an effective enzyme-immobilizing material.[15–18] Most prevalent in the literature, enzyme-immobilized silk films have been successfully used in several biosensors for glucose and hydrogen peroxide detection.[15] Silk-based biosensors were able to be used to analyze various biosamples, including human whole blood or serum, over two years and were useful for up to two years post enzyme embedding.[18] Such reports confirm our finding that silk fibroin films may be incorporated with labile bioactive molecules whereupon they remain active within the bulk silk material region. More recent accounts have shown that heme-proteins, such as hemoglobin and myoglobin, may be embedded within a silk fibroin matrix to act as electron transfer agents upon a graphite electrode surface with nearly reversible cyclic voltammetric peaks.[17] Such studies provide evidence that bioactive charge carriers, such as heme-proteins, may be embedded within the silk matrix and retain function. This approach to embedding charge carrying structures could be combined with the outstanding optical properties of silk demonstrated in the present study, for uses in electro-optical charge transfer applications.

These results exemplify a new generation of optical elements that exploit the unique material features and processing of silk proteins to incorporate biological "sensors" within the optical element. Nanopatterned optical silk fibroin gratings integrate the methodologies of optical physics with biomaterials, to generate new opportunities in detection and sensing. The noteworthy trait of these examples is the ability to embed and maintain biological activity within a structured and robust material across varying "biological scales", encompassing small organics, complex proteins such as hemoglobin, and enzymes such as peroxidase.

Additionally, an important feature of these devices is their full biodegradability and biocompatibility.[2,4,19] Silks degrade via proteolytic activity via surface erosion, and we have previously shown the ability to track the rates of such degradation in both silk fibers and films.[8] Because of these features, the application space can decisively shift into the environmental and life sciences where these features are paramount. The refined optical functions obtainable through nanopatterning would be then available for a class of new devices that could unobtrusively enter and monitor a natural environment, such as the human body. For example, devices for implantation in vivo become feasible, without a need to retrieve the system at a later point, and the degradation lifetime can be programmed based on the processing used. Devices that can be dispersed in the environment, again without the need to retrieve them at a later time point, also establish novel and useful platforms for remote sensing and detection systems.

Conclusion

We have demonstrated that processing the silk protein at room temperature in water, with control of physical cross-links, allows for the formation of materials with high optical clarity while realizing sophisticated diffractive structures ranging from lenses or predefined one or two-dimensional light patterns. These diffractive optical elements can also be functionalized to maintain biologically active optical elements. This integration allows the use of patterned optical surfaces to deliver light within a biological matrix and provide optimal coupling of photons

with the doped substrate to probe biological function or to generate designed optical discrimination, interface or readout. The availability of a biological matrix, such as silk, that has the material toughness for "ordinary" environmental conditions while simultaneously exhibiting high optical quality and biological activity is unique and should pave the way to a new generation of optical filters, biosensors, active materials, waveguides and all-optical biodetectors. This anticipated future set of outcomes is based on the relative ease of materials formation, the use of ambient processing conditions, and the retention of biological and optical functions during the preparation and storage process for these materials.

Acknowledgment. This work was funded by the NIH, the NSF, and the AFOSR. We acknowledge Sergio Fantini for useful discussions and comments and Jessica Wargats (Digital Optics Inc., Tessera Corporation) for providing the polycarbonate cards with the diffractive optics.

References and Notes

(1) (a) Marshall, A J.; Blyth, J.; Davidson, C. A. B. *Anal. Chem.* **2003**, *75* (17), 4423. (b) Lee, M. C.; Kabilan, S.; Hussain, A. *Anal. Chem.* **2004**, *76* (19), 5748. (c) Sartain, F. K.; Yang, X. P.; Lowe, C. R. *Anal. Chem.* **2006**, *78* (16), 5664.

(2) Park, U.-J.; Kim, J.; Li, C.; Jin, H-J.; Valluzzi, R.; Kaplan, D. L. *Biomacromolecules* **2004**, *5*, 786.

(3) Meinel, V.; Karageorgiou, L.; Hofmann, S.; Malhotra, A.; Volloch, V.; Schwob, J.; Kaplan, D. L. *J Biomed. Mater. Res* **2004**, *71A*, 528. (a) Sofia, S.; McCarthy, M. B.; Gronowicz, G.; Kaplan, D. *J. Biomed. Mater. Res.* **2001**, *54* (1), 139. (b) Karageorgiou, V.; Tomkins, M.; Fajardo, R.; Meinel, L.; Snyder, B.; Wade, K.; Chen, J.; Vunjak-Novakovic, G.; Kaplan, D. L. *J. Biomed. Mater. Res., Part A* **2006**, *78* (2), 324. (c) Wang, M.; Jin, H. J.; Kaplan, D. L.; Rutledge, G. C. *Macromolecules* **2004**, *37* (18), 6856. (d) Wang, X. Y.; Kim, H. J.; Xu, P.; Matsumoto, A.; Kaplan, D. L. *Langmuir* **2005**, *21* (24), 11335.

(4) Jin, H.-J.; Park, J.; Karageorgiou, V.; Kim, U.-J.; Valluzzi, R.; Cebe, P.; Kaplan, D. L. *Adv. Funct. Mater.* **2005**, *15* (8), 1241.

(5) Jiang, C.; Wang, X.; Gunawidjaja, R.; Lin, Y-H.; Gupta, M. K.; Kaplan, D. L.; Naik, R. R.; Tsukruk, V. V., *Adv. Funct. Mater.* **2007**, *17*, 2229.

(6) Gupta, M. K.; Khokar, S. K.; Phillips, D. M.; Sowards, L. A.; Drummy, L. F.; Kadakia, M. P.; Naik, R. R. *Langmuir* **2007**, *23*, 1315.

(7) Diaz, G. H.; Altman, F.; Jakuba, C.; Calabro, T.; Horan, R. L.; Chen, J.; Lu, H.; Richmond, J.; Kaplan, D. L. *Biomaterials* **2003**, *24*, 401.

(8) Jin, H. J.; Fridrikh, S. V.; Rutledge, G. C.; Kaplan, D. L. *Biomacromolecules* **2002**, *3* (6), 1233.

(9) (a) Omenetto, F. G.; Wolchover, N. A.; Wehner, M. R.; Ross, M.; Efimov, A.; Taylor, A. J.; Kumar, V. V. R. K.; George, A. K.; Knight, J. C.; Joly, N. Y.; Russell, P. St. J. *Opt. Express* **2006**, *14* (11), 4928. (b) Russell, P. *Science* **2003**, *299* (5605), 358. (c) Wadsworth, W. J.; Ortigosa-Blanch, A.; Knight, J. C.; Birks, T. A.; Man, t.-P. M.; Russell, P. St. J. *J. Opt. Soc. Am. B* **2002**, *19* (9), 2148.

(10) (a) Llewellynsmith, I. J.; Pilowsky, P.; Minson, J. B. *J. Neurosci. Methods* **1993**, *46* (1), 27. (b) Weinberg, R. J.; Vaneyck, S. L. *J. Histochem. Cytochem.* **1991**, *39* (8), 1143.

(11) (a) Xia, Y. N.; Kim, E.; Whitesides, G. M. *Chem. Mater.* **1996**, *8* (7), 1558. (b) Xia, Y. N.; Kim, E.; Zhao, X. M.; Rogers, J. A.; Prentiss, M.; Whitesides, G. M. *Science* **1996**, *273* (5273), 347.

(12) Gupta, M. K.; Khokhar, S. K.; Phillips, D. M.; Sowards, L. A.; Drummy, L. F.; Kadakia, M. P.; Naik, R. R. *Langmuir* **2007**, *23* (3), 1315.

(13) (a) Horecker, B. L. *J. Biol. Chem.* **1943**, *148* (1), 173. (b) Wray, S.; Cope, M.; Delpy, D. T.; Wyatt, J. S.; Reynolds, E. O. R. *Biochim. Biophys. Acta* **1988**, *933* (1), 184. (c) Petrich, J. W.; Poyart, C.; Martin, J. L. *Biochemistry* **1988**, *27* (11), 4049.

(14) Vepari, C.; Kaplan, D. L. *Biotechnol. Bioeng.* **2006**, *93*, 1130.

(15) (a) Demura, M.; Asakura, T. *Biotechnol. Bioeng.* **1989**, *33* (5), 598. (b) Demura, M.; Asakura, T. *J. Membr. Sci.* **1991**, *59* (1), 39. (c) Miyairi, S.; Sugiura, M.; Fukui, S. *Agric. Biol. Chem.* **1978**, *42* (9), 1661.

(16) Demura, M.; Asakura, T.; Nakamura, E.; Tamura, H. *J. Biotechnol.* **1989**, *10* (2), 113.

(17) Wu, Y.; Shen, Q.; Hu, S. *Anal. Chim. Acta* **2006**, *558* (1–2), 179.

(18) Zhang, Y. Q. *Biotechnol. Adv.* **1998**, *16* (5–6), 961.

(19) Horan, R. L.; Antle, K.; Collette, A. L.; Wang, Y.; Huang, J.; Moreau, J. E.; Volloch, V.; Kaplan, D. L.; Altman, G. H. *Biomaterials* **2005**, *26* (17), 3385.

BM701235F